BIOCHEMISTRY
including biophysical chemistry & molecular biology
Article

Biochemistry **2009,** *48,* 5121–5130 5121
DOI: 10.1021/bi9001387

Redox-Dependent Conformational Changes in Cytochrome *c* Oxidase Suggest a Gating Mechanism for Proton Uptake[†,‡]

Ling Qin,[§] Jian Liu, Denise A. Mills, Denis A. Proshlyakov, Carrie Hiser, and Shelagh Ferguson-Miller*

Biochemistry and Molecular Biology Department, Michigan State University, East Lansing, Michigan 48824
[§]Present address: Department of Biomass Science and Conversion Technology, Sandia National Laboratories, Livermore, CA 94551

Received January 28, 2009; Revised Manuscript Received April 23, 2009

ABSTRACT: A role for conformational change in the coupling mechanism of cytochrome *c* oxidase is the subject of controversy. Relatively small conformational changes have been reported in comparisons of reduced and oxidized crystal structures of bovine oxidase but none in bacterial oxidases. Comparing the X-ray crystal structures of the reduced (at 2.15 Å resolution) and oxidized forms of cytochrome *c* oxidase from *Rhodobacter sphaeroides*, we observe a displacement of heme a_3 involving both the porphyrin ring and the hydroxyl farnesyl tail, accompanied by protein movements in nearby regions, including the mid part of helix VIII of subunit I which harbors key residues of the K proton uptake path, K362 and T359. The conformational changes in the reduced form are reversible upon reoxidation. They result in an opening of the top of the K pathway and more ordered waters being resolved in that region, suggesting an access path for protons into the active site. In all high-resolution structures of oxidized *R. sphaeroides* cytochrome *c* oxidase, a water molecule is observed in the hydrophobic region above the top of the D path, strategically positioned to facilitate the connection of residue E286 of subunit I to the active site or to the proton pumping exit path. In the reduced and reduced plus cyanide structures, this water molecule disappears, implying disruption of proton conduction from the D path under conditions when the K path is open, thus providing a mechanism for alternating access to the active site.

Cytochrome *c* oxidase (C*c*O)[1], the terminal enzyme of the electron transfer chain, provides the final electron sink by accepting electrons from reduced cytochrome *c* and passing them sequentially through Cu_A, heme *a*, and finally to its active site, composed of heme a_3 and Cu_B. Oxygen binds at this binuclear center, accepts the electrons, and is reduced to water. The energy released from oxygen reduction is utilized by C*c*O to translocate protons from the N-side (negative side) of the membrane to the P-side (positive side), to generate an transmembrane proton electrochemical gradient, which is then used for ATP synthesis (for recent reviews, see refs (*1*−*3*)). Extensive kinetic and spectroscopic studies have identified intermediate states during the chemical catalysis, yet the details of the oxygen reduction process are not entirely understood. Even more elusive and controversial is the proton pumping mechanism.

Two types of protons, termed pump and substrate protons, are taken up from the N-side of the membrane. During each catalytic cycle, four pump protons are translocated to the P-side of the membrane, while four substrate protons are used in the oxygen reduction to water. Previous studies on bacterial C*c*O have identified two proton uptake pathways, D and K, within the transmembrane portion of the enzyme (*4*, *5*). They are named after key residues in each pathway, $D132_I$ and $K362_I$ (*Rhodobacter sphaeroides* (*Rs*) C*c*O numbering, with the subscript representing the subunit), respectively. These two pathways contain crystallographically resolved water molecules which, together with polar residues, enable proton conduction (*4*, *6*, *7*).

The D path is considered to transport all of the pump protons, as well as at least two substrate protons (*8*, *9*). In the high-resolution crystal structures of *Rs*C*c*O, a clear chain of hydrogen-bonded water molecules is resolved in the vicinity of the D pathway, between $D132_I$ and $E286_I$ (*6*, *7*). The latter residue is considered to be the branching point beyond which a proton is

[†]This work is supported by National Institutes of Health Grants GM26916 (S.F.-M.) and GM070544 (D.A.P.), Michigan State University Research Excellence Fund Grant 03-016 (S.F.-M.), and Michigan Technology Tri-Corridor Center for Structural Biology Core Technology Alliance Grant 085P1000817.

[‡]The atomic coordinates and structure factors of reduced and cyanide-bound reduced *R. sphaeroides* cytochrome *c* oxidase have been deposited in the Protein Data Bank with access codes of 3FYE and 3FYI, respectively.

*To whom correspondence should be addressed. Phone: 517-355-0199. Fax: 517-353-9334. E-mail: fergus20@msu.edu.

[1]Abbreviations: C*c*O, cytochrome *c* oxidase; *Rs*, *Rhodobacter sphaeroides*; I−II *Rs*C*c*O, the form of *Rs*C*c*O containing the catalytic core subunits I and II; *Pd*, *Paracoccus denitrificans*; PDB, Protein Data Bank; ATP, adenosine triphosphate; PEG-400, polyethylene glycol with an average molecular weight of 400; MES, 2-(*N*-morpholino)ethanesulfonic acid; HEPES, 4-(2-hydroxyethyl)piperazine-1-ethanesulfonic acid; TMPD, *N*,*N*,*N*′,*N*′-tetramethyl-*p*-phenylenediamine; MD, molecular dynamics. Unless otherwise noted, the amino acid numbering of cytochrome *c* oxidase in this report is from *R. sphaeroides*, with the subscript representing the subunit number.

 Published on Web 04/27/2009

either translocated to the outside of the membrane via an unidentified route or transported to the binuclear center for oxygen reduction to water (*10*, *11*).

Evidence suggests that the K path is used for transporting one to two substrate protons during the reductive half of the oxygen chemistry cycle (O → R) (*12*, *13*). The path is considered to start with E101 of subunit II (*14*) (but see ref *15*) and involve key residues $S299_I$, $K362_I$, and $T359_I$, the latter two located in the middle part of helix VIII of subunit I. The mutation of these residues leads to a major loss of activity, up to 99.95% for K362 M (*5*, *16*). Compared with the D path, there are very few water molecules resolved, only two in the available crystal structures so far. One is hydrogen bonded to $K362_I$ and $S299_I$, the other to $T359_I$ and the OH group of the heme a_3 hydroxylfarnesyl tail (heme a_3 farnesyl−OH) (*6*, *7*). The latter group also forms a strong hydrogen bond with the OH group of $Y288_I$ ($Y288_I$−OH), which has a unique covalent bond between the side-chain atoms with the Cu_B ligand $H284_I$ in the active site. The strong hydrogen bonding between $Y288_I$−OH and heme a_3 farnesyl−OH (O−O distance of 2.6 Å) is proposed to function as a closed K path gate, since its presence prohibits proton transport via that path to the active site (*17*, *18*). This fits with the hypothesis that in the oxidized state the K path is expected to be closed (*19*). No water molecules are resolved between $Y288_I$ and the binuclear center in all of the oxidized C*c*O crystal structures, even at high resolution.

In this paper, we report the structure of the dithionite-reduced form of *Rs*C*c*O, a bacterial enzyme highly homologous to the mammalian mitochondrial C*c*O. The structure shows a significant displacement of heme a_3, leading to the loss of the strong hydrogen bond between Y288−OH and heme a_3 farnesyl−OH, the movement of the middle part of helix VIII that contains key residues of the K path, and appearance of resolved water molecules leading from the top of the K path into the binuclear center. These observed changes, along with the loss of a water molecule above the D path, suggest conformational control of alternate opening of the K and D paths for proton transport to the active site.

MATERIALS AND METHODS

Protein Expression, Purification, and Crystallization of RsCcO. In order to obtain I−II *Rs*C*c*O crystals, *Rs* cells (strain 37Δ4 (*7*)) were grown and harvested, and membrane samples were prepared as described (*20*). The protein purification and crystallization procedure were described earlier (*7*). In order to obtain four subunit *Rs*C*c*O crystals, *Rs* strain 169 was generated by transferring plasmid pCH169 (*7*) into *Rs* strain YZ200 (*20*). The growth and harvest of the cells and preparation of plasma membranes were described earlier (*20*). The protein purification and crystallization procedure for four subunit *Rs*C*c*O were described earlier (*21*).

Treatments of RsCcO Crystals To Produce the Reduced Form and the Cyanide-Bound Reduced Form. Prior to flash cooling, crystals of *Rs*C*c*O were soaked in a stabilizing solution containing 91 mM MES, pH 6.3, 18.2 mM Tris, pH 8.0, 91 mM NaCl, 30 mM $MgCl_2$, 2 mM $CdCl_2$, 0.16% decyl maltoside, 0.013% dodecyl maltoside, 4.4% 1,2,3-heptanetriol, and 24% (v/v) PEG-400, supplemented with 10 mM sodium dithionite. The crystals were soaked for 5−10 min at 4 °C to reduce the crystals. The C*c*O crystals turned green within a few minutes and remained green throughout the entire process. The surrounding solution was gradually exchanged into the cryosolution that contained the same ingredients as in the stabilizing solution except for a higher concentration (32%) of PEG-400, also supplemented with 10 mM sodium dithionite. The crystals were then picked and flash cooled in liquid nitrogen.

To produce cyanide-bound reduced *Rs*C*c*O crystals, the crystals were first reduced as described above by adding stabilizing solution supplemented with 10 mM dithionite. The surrounding stabilizing solution was then exchanged into a new stabilizing solution supplemented with 10 mM dithionite and 20 mM cyanide. The crystals were soaked in this solution for another 5 min. The surrounding solution was then gradually exchanged into cryosolution with 32% PEG-400, also supplemented with 10 mM dithionite and 20 mM cyanide. The cyanide-bound reduced crystals were then flash cooled in liquid nitrogen.

Removal of Cd from I−II RsCcO Crystals. Crystals of I−II *Rs*C*c*O were soaked in stabilizing solution as described earlier, except that no Cd was present, for 1 h. The soaking solution was then exchanged into a fresh stabilizing solution containing 10 mM dithionite, still without Cd, for another 45 min. The stabilizing solution was then slowly exchanged into the Cd-free cryosolution supplemented with dithionite as described earlier, prior to flash cooling in liquid nitrogen.

Reoxidation of the Reduced RsCcO Crystal. Crystals of I−II *Rs*C*c*O were reduced with 10 mM dithionite as described above. The soaking solution was then exchanged into a stabilizing solution with no dithionite. The soaking solution free of dithionite was then slowly exchanged into cryosolution containing 32% PEG-400, with no dithionite and supplemented with 1 mM ferricyanide. The crystals turned from green to brownish red during the exchanging process, which took approximately 5 min. The reoxidized crystals were soaked in the cryosolution with ferricyanide for another 5 min prior to being flash cooled in liquid nitrogen.

X-ray Crystallographic Data Collection and Structural Refinement. X-ray diffraction data of the dithionite-reduced, as well as Cd-free reduced, I−II *Rs*C*c*O crystals were collected at Station 23-ID-B, GM/CA-CAT, Advanced Photon Source, Argonne National Laboratory. Diffraction data from the cyanide-bound reduced form, as well as the reduced/reoxidized form of I−II *Rs*C*c*O crystals, were collected at Station 21-ID-G, LS-CAT, Advanced Photon Source, Argonne National Laboratory. The data were processed with HKL2000 (*22*), and the structures were solved by molecular replacement using the oxidized I−II subunit *Rs*C*c*O (PDB entry 2GSM (*7*)) as the starting model and refined by Refmac5 (*23*) from the CCP4 program suite (*24*). Molecular visualization and model building were performed using the program COOT (*25*). The refinement statistics for the final models of reduced and cyanide-bound reduced I−II *Rs*C*c*O are presented in Table 1. All figures with molecular models were generated using the program PYMOL (DeLano Scientific).

The diffraction data for the reduced four subunit *Rs*C*c*O crystal were collected at station 21-ID-D, LS-CAT, Advanced Photon Source, Argonne National Laboratory. The crystal diffracted anisotropically to approximately 3.2 Å resolution. The structure was determined by molecular replacement using the published oxidized four subunit *Rs*C*c*O structure (PDB entry 1M56 (*6*)) as the starting model and refined using CNS1.1 (*26*).

In order to confirm the loss of Cd at the $E101_{II}$ site for the Cd-free reduced I−II *Rs*C*c*O crystal, anomalous diffraction data were collected at station 23-ID-B, GM/CA-CAT, Advanced Photon Source, Argonne National Laboratory. The wavelength

Table 1: Data Collection and Refinement Statistics of Reduced and Cyanide-Bound Reduced *Rs*C*c*O

	dithionite reduced	cyanide-bound dithionite reduced
	(A) Unit Cell Parameters	
space group	$P2_12_12_1$	$P2_12_12_1$
cell dimensions (Å)	a = 124.6, b = 131.5, c = 176.2	a = 124.3, b = 131.9, c = 176.2
molecules per asym unit	2	2
	(B) Data Collection	
resolution range (Å)	50−2.15 (2.15−2.206)[a]	50−2.2 (2.20−2.257)[a]
completeness (%)	99.1 (92.7)[a]	96.2 (73.5)[a]
no. of unique reflections	151414 (10311)[a]	137425 (7652)[a]
redundancy	4.6 (4.0)[a]	6.7 (3.7)[a]
R_{merge}[b] (%)	6.5 (60.6)[a]	7.2 (52.0)[a]
I/σ	20.8 (1.8)[a]	20.3 (1.9)[a]
	(C) Structural Refinement	
no. of refined atoms	13615	13605
R-factor[b]/R_{free} (%)	19.6/22.1 (27.4/29.5)[a]	19.4/21.9 (25.5/30.1)[a]
average B-factor	45.8	44.0
rmsd bond length (Å)	0.012	0.011
rmsd bond angle (deg)	1.227	1.155

[a] Highest resolution shell. [b] $R_{merge} = \sum|I_h - \langle I_h\rangle|/\sum I_h$ over all h, where I_h is the intensity of reflection h. R-factor $= \sum||F_o| - |F_c||/\sum|F_o|$, where F_o and F_c are the observed and calculated structure factors, respectively. A randomly selected subset of the data (3%, approximately 4000 reflections) was used to calculate R_{free}.

of the X-ray was set at 1.984 Å, where cadmium has a strong anomalous signal. The published oxidized two subunit *Rs*C*c*O structure (PDB entry 2GSM (*7*)) was used as the starting phasing model in a rigid body refinement, and the anomalous difference Fourier map was calculated with the CCP4 program suite (*24*) using the phases of the rigid-body refined structure. In order to minimize bias, all metals in the structure were removed from the phase calculation.

Spectral Studies of Irradiated Reduced RsCcO Crystals. Optical absorption measurements in crystals were carried out using a fiber optics spectrometer (model S2000; Ocean Optics). One end of a 50 μm optical fiber was attached to the spectrometer while the other end was fixed pointing upward (for detailed setup, see Figure S1 of the Supporting Information). A short length of tubing was placed over the fiber termination ferrule (3.2 mm diameter) forming a sample dish ~1 mm deep. Transmission light was provided by a tungsten lamp, which was offset from the optical fiber axis by 40° at a distance of approximately 50 cm. A paper diffuser (10 cm diameter) located 2 cm above the sample dish provided a uniform, broad-angle light illumination source. Only the light scattered by the diffuser, but not the direct light from the lamp, could be collected by the 25° (in the air) acceptance angle of the optical fiber. No other light sources were present. The sample dish was filled with the cryoprotectant buffer for reference measurements (150 s). While the diffuser was removed, a previously reduced and irradiated crystal from liquid nitrogen was placed in the buffer, and a microscope was used to position the crystal directly above the optical fiber. Sample measurements were started immediately after repositioning the diffuser, and spectra were recorded continuously every 0.2 s and averaged in 30 s intervals throughout the experiment. Configuration with a diffuse probe light showed little sensitivity to the loss of light due to refractivity and scattering on crystal surfaces and protein aggregates.

Online Single-Crystal Microspectroscopy. The online single-crystal microspectrophotometer available at station 14-BM-C, BioCARS, Advanced Photon Source, Argonne National Laboratory, was used to record the spectrum of the CN-bound reduced I−II *Rs*C*c*O frozen crystal. The assembly of the equipment is described in detail elsewhere (*27*). Due to the anisotropic arrangements of chromophores in protein crystals, which can lead to large spectral distortion depending upon the crystal orientation, the crystal was carefully aligned so that the resulting spectrum resembles the isotropic solution spectrum.

Oxidase Activity Assay. Measurements of the rates of O_2 reduction were performed at 25 °C using an oxygen electrode. For assay at pH 6.2, the reaction mixture (total volume 1.8 mL) contained 50 mM MES−KOH, pH 6.2, 19 mM KCl, 2.8 mM ascorbate, 1.1 mM TMPD, 0.1% dodecyl maltoside, 6.7 nM C*c*O, and 30 μM horse heart cytochrome *c*. For assay at pH 7.4, the reaction mixture contained 50 mM HEPES, pH 7.4, 24 mM KCl, 2.8 mM ascorbate, 1.1 mM TMPD, 0.1% dodecyl maltoside, 6.7 nM C*c*O, and 30 μM horse heart cytochrome *c*.

RESULTS

Displacement of Heme a_3 in the Reduced RsCcO Structure. The crystal structure of the dithionite-reduced *Rs*C*c*O was determined at 2.15 Å resolution (see Table 1 for data collection and refinement statistics). The reduced *Rs*C*c*O shows no significant conformational changes in the overall structure of the enzyme except in regions near the active site, most notably in the heme a_3 moiety. In comparison to the oxidized structure (PDB entry 2GSM) (*7*), the heme a_3 porphyrin ring rotates 6−8° about the carboxyl group of the A-ring propionate, as seen from the direction of Cu_B (Figure 1). This rotation is accompanied by a subtle tilt of the plane of the porphyrin ring. The continuous electron density between the two metals of the binuclear center in the oxidized structure (Figure 2A), tentatively assigned to be a water and a OH^- bound to Fe−a_3 and Cu_B, respectively (*7*), is gone. The absence of the bridging ligands was also observed in the reduced C*c*O structures from *Paracoccus denitrificans* (*Pd*) (*28*), bovine (*29*), and *Thermus thermophilus* (*30*). Therefore, it appears that in the fully reduced state (R state) the two product

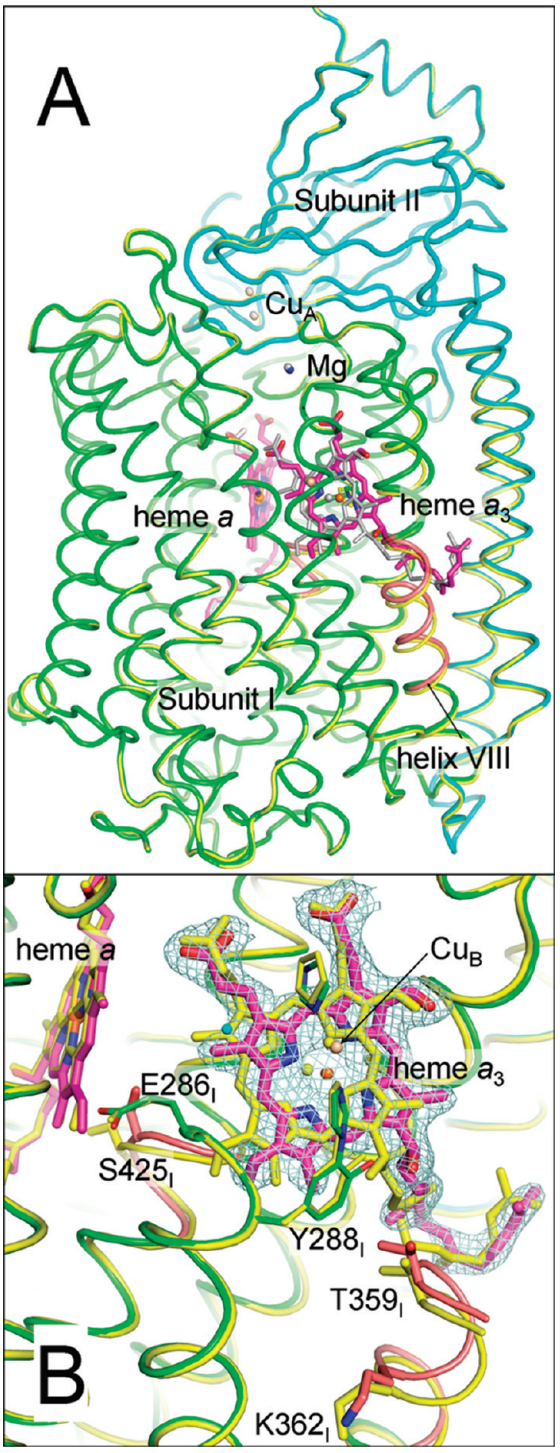

FIGURE 1: Comparison of *Rs*C*c*O structure between the reduced and oxidized states. (A) Overall structure of I−II subunit *Rs*C*c*O. In the reduced structure, the protein backbone is displayed in cartoon and colored by different subunits (subunit I, green; subunit II, cyan), and the heme groups, *a* and a_3, are shown in sticks and colored by atom type (C, magenta; O, red; N, blue). The metals in the reduced structure are displayed in spheres and colored differently (Fe, orange; Cu, wheat; Mg, blue). In the oxidized structure, the protein subunits are colored yellow, and the heme groups and metals are colored gray. Two patches of peptides in the reduced structure, where significant conformational changes are observed compared with those in the oxidized structure, are shown in deep salmon. (B) Structure at the active site region. The reduced structure is colored in the same manner as in (A), while that of the oxidized structure is colored yellow. The $2F_o - F_c$ difference Fourier map contoured at the 1.0σ level is colored light blue. Several key residues in the structures are displayed in sticks and colored by atom type in the reduced structure and yellow in the oxidized structure.

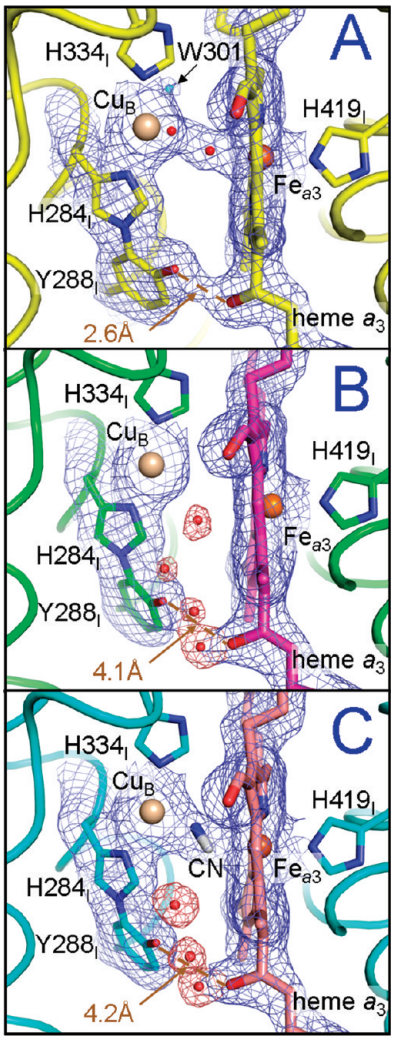

FIGURE 2: Structural comparison of the active site in the oxidized (A), reduced (B), and cyanide-bound reduced (C) states of *Rs*C*c*O. (A) In the oxidized structure, the protein backbone is colored yellow; heme a_3 and several key residues in the active site region are displayed as sticks and colored by atom type (C, yellow; O, red; N, blue). The metals Fe_{a_3} and Cu_B are displayed as spheres and colored orange and wheat, respectively. The two bridging ligands between Cu_B and Fe_{a_3}, temporarily assigned as an OH^- ligated to Cu_B and a water ligated to Fe, are displayed as small red spheres. The water molecule (W301) resolved in the hydrophobic region near the binuclear center between the top of the D path and the binuclear center is displayed as a cyan sphere. $2F_o - F_c$ difference Fourier map contoured at 1.0σ is colored blue. (B) In the reduced structure, the protein backbone is colored green, several key residues in the active site region are colored by atom type (C, green; O, red; N, blue), and heme a_3 is colored by a different color scheme (C, magenta; O, red; N, blue). The metals are displayed in the same manner as in (A), and additionally resolved water molecules in the reduced structure are displayed in small red spheres. $2F_o - F_c$ difference Fourier map surrounding the binuclear center, contoured at 1.0σ, is colored blue, and that surrounding the additionally resolved water molecules is colored red. (C) In the cyanide-bound reduced structure, the protein backbone is colored cyan, several key residues in the active site region are colored by atom type (C, cyan; O, red; N, blue), and heme a_3 is colored by a different color scheme (C, salmon; O, red; N, blue). The metals and additionally resolved water molecules in the reduced structure are displayed in the same manner as in (B). The cyanide molecule is displayed as sticks and colored by atom type (C, gray; N, blue). $2F_o - F_c$ difference Fourier map is displayed in the same manner as in (B). In all structures, the O−O distance between the $Y288_I$−OH and the OH group of the heme a_3 hydroxyl farnesyl tail is represented by the brown dashed line and labeled.

water molecules are no longer bound to the binuclear center metals, consistent with results from the resonance Raman spectroscopic studies which show the Fe−a_3 is five coordinated in the reduced state (*31*). Due to the missing bridging ligands in the binuclear center, the Fe^{2+} atom is more out of the plane of the porphyrin ring, moved toward the $His419_I$ ligand, and the distance between Fe^{2+}−a_3 and Cu_B^{1+} becomes larger (5.4 Å in the reduced state compared to 4.9 Å in the oxidized state) (Figure 2B) (Table S1 of the Supporting Information). Besides the movement of the porphyrin ring, the hydroxylfarnesyl tail undergoes significant rotational movement, which widens the distance between the heme a_3 farnesyl−OH and $Y288_I$−OH from a tight hydrogen-bonding distance of 2.6 Å in the oxidized structure (Figure 2A) to approximately 4.1 Å in the reduced structure (Figure 2B) (Table S1 of the Supporting Information).

Moreover, compared with the oxidized structure (Figure 2A), there are four more water molecules clearly resolved in the region, including one that sits between the now separated $Y288_I$−OH and heme a_3 farnesyl−OH, as shown in Figure 2B. These additional water molecules provide a hydrogen-bonded water chain, connecting the upper part of the K path to the binuclear center.

Movements in the Protein in the Reduced RsCcO Structure. The conformational change in heme a_3 is accompanied by significant movement of the protein in nearby regions, especially the mid part of helix VIII (shown in Figure 1A), involving residues 355−364 of subunit I (Figure 1). On the distal side of the heme a_3 plane, in the angle between the porphyrin rings of heme *a* and a_3, additional movement of the protein is observed involving residues 423−426 of helix X (Figure 1B). The conformational change of $S425_I$ is the most striking: not only is the main-chain Cα atom moved 2.9 Å in the reduced structure, its side-chain OH group points in the opposite direction from that in the oxidized form. Similar movements in these residues were also seen in the reduced bovine C*c*O structure (see Discussion). Not seen in the bovine C*c*O, a few residues on the other side of heme a_3 are moved, in helix IX of *Rs*C*c*O centered on $Ile399_I$, accommodating the heme a_3 ring and tail displacement toward them.

Structure of the Cyanide-Bound Reduced RsCcO. Cyanide binds at the active site of cytochrome oxidase and prevents oxygen binding, hence its potent toxic effect on cellular metabolism (*32*). The structure of the CN-bound, reduced *Rs*C*c*O was solved at 2.2 Å resolution (see Table 1 for data collection and structural refinement statistics). The binding of CN to reduced *Rs*C*c*O was confirmed by the absorption spectrum of the frozen crystal before X-ray irradiation (Figure 3), obtained at station 14-BM-C, BioCARS, Advanced Photon Source, Argonne National Laboratory, using their custom-built online single-crystal microspectrometer setup as described (*27*). The spectrum shows the expected broadened α peak in the 590−606 region (*33*) (in contrast to the reduced C*c*O spectrum, Figure 6). Compared with the reduced active site with no bridging ligand (Figure 2B, the CN molecule was clearly resolved between the two metals, shown in Figure 2C. It is noteworthy that although previous studies on bovine C*c*O have suggested two CN binding interactions at the binuclear center (*34*), our crystal structure of CN-bound *Rs*C*c*O only reveals one binding geometry, likely representing only the predominant form under our experimental conditions. The same displacement of the porphyrin ring of heme a_3, together with the movement of the mid part of helix VIII seen in reduced structure without CN, is also observed in the CN-bound, reduced structure. However, due to strong interaction between the carbon ion of CN and Fe−a_3, the Fe^{2+} has moved back toward the plane of the porphyrin ring and the distance between Cu_B and Fe−a_3 is approximately 5.0 Å, similar to that in the oxidized structure. Moreover, there are only three, rather than four, additional waters resolved between the top of the K path and the active site, with the one closest to the active site missing (Figure 2B,C).

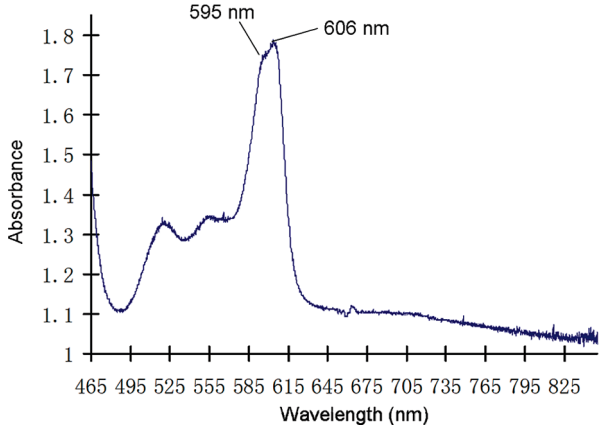

FIGURE 3: Spectrum of the CN-bound reduced *Rs*C*c*O crystal. The spectrum was taken of the frozen crystal before irradiation at 100 K at beamline 14-BM-C, BioCARS, Advanced Photon Source, as described in Materials and Methods.

Structure of the D Pathway in the Reduced State. In contrast to the structure of the K path, there are no major protein conformational changes observed in the D path in the reduced vs oxidized state. As shown in Figure 4, there is no difference in the ordered, hydrogen-bonded water network connecting the vicinity of $D132_I$ to the vicinity of $E286_I$ or in the aligning residues. The only significant change in the D path region between the reduced and oxidized structure is in the hydrophobic area between $E286_I$ and the active site. In the oxidized structure, there is a water molecule (W301) resolved in this location. This water disappears in the reduced structure and in the reduced CN-bound form. The potential significance of this change is further elaborated later (see Discussion).

Structure of Reduced RsCcO with No Cd Bound to $E101_{II}$ at the K Path Entrance. Cadmium is an essential ingredient in our crystallization experiments because it mediates intermolecular crystal contacts (*7*). Similar to Zn, it is also an known inhibitor of C*c*O (*35*, *36*). One of the inhibitory binding sites is at the entrance of the K path, $E101_{II}$ (*21*). In fact, cadmium is found bound to $E101_{II}$ and $H96_{II}$ in our I−II subunit *Rs*C*c*O structures in both oxidized and reduced forms. It is conceivable that the structural changes observed in this work are somehow related to the fact that the enzyme is inhibited in the K path during dithionite reduction. In order to test this possibility, a number of crystals were soaked in a Cd-free stabilizing solution for different periods of time, followed by dithionite reduction. The data collection on these crystals was performed at the selected wavelength of 1.974 Å (6250 eV) where Cd has a strong anomalous signal, and the presence of Cd at the $E101_{II}$ site was checked by an anomalous difference Fourier map. Soaking in Cd-free solution led to Cd dissociation both at the $E101_{II}$ site and at the crystal contact region; the diffraction limit of these reduced crystals deteriorated significantly to only 3.3 Å. Nevertheless, it was found that a 1 h soaking in Cd-free stabilizing solution followed by a 45 min soaking with stabilizing solution supplemented with dithionite completely removed the Cd binding at the $E101_{II}$ site, as evidenced by the disappearance of the intense peak

in the anomalous difference Fourier map. The C*c*O crystal structure with no Cd at the $E101_{II}$ site still showed the displacement of heme a_3 and regions in helix VIII, as described earlier. Due to the lower diffraction resolution limit, we were unable to confirm the presence of the additional water molecules between $T359_I$ and the binuclear center; however, it is reasonable to conclude that the conformational changes we see in this study are not a result of the inhibitory binding of Cd at $E101_{II}$ site.

This conclusion is reinforced by studies with the four-subunit crystal that is produced in the absence of Cd. This crystal form diffracts to lower resolution than the two-subunit enzyme crystal; the reduced state was solved at a resolution of 3.2 Å. Although the structure is not of the resolution to reveal all atomic details, it still clearly shows the key findings of this work, including the displacement of heme a_3, as evidenced by the widening of the distance between $Y288_I$−OH and heme a_3 farnesyl−OH (Table S1 of the Supporting Information), as well as the main-chain movement of the mid part of helix VIII. The result confirms that neither the presence of Cd nor the absence of subunit III is responsible for the observed conformational changes.

Reversibility of the Conformational Changes in Reduced RsCcO. In order to test whether the conformational changes in the reduced structure were reversible, a reduced I−II *Rs*C*c*O crystal was subjected to reoxidation by ferricyanide, and the structure of the reoxidized crystal was determined. The reduced and then reoxidized structure is essentially the same as that of the oxidized, with all the conformational changes in the heme a_3 group, as well as in the protein moiety returned to the oxidized state (Table S1 of the Supporting Information).

Biochemical Characterization of Redissolved, Reduced I−II RsCcO Crystals. The redissolved reduced crystals of I−II *Rs*C*c*O have a normal UV−visible spectrum, as shown in Figure 5A, as well as normal oxidase activity measured using an oxygen electrode, as shown in Figure 5B. The redissolved reduced I−II *Rs*C*c*O crystals show suicide inactivation, typical for C*c*O lacking subunit III (*37*), which can be rescued by lower pH (*37*) (Figure 5B). This effect is also seen in the redissolved oxidized crystals (*7*). The results show that no irreversible structural change has been caused by the conditions of crystallization or reduction.

Spectral Characterization of RsCcO Crystals after X-ray Irradiation. It is well-known that exposure to X-ray

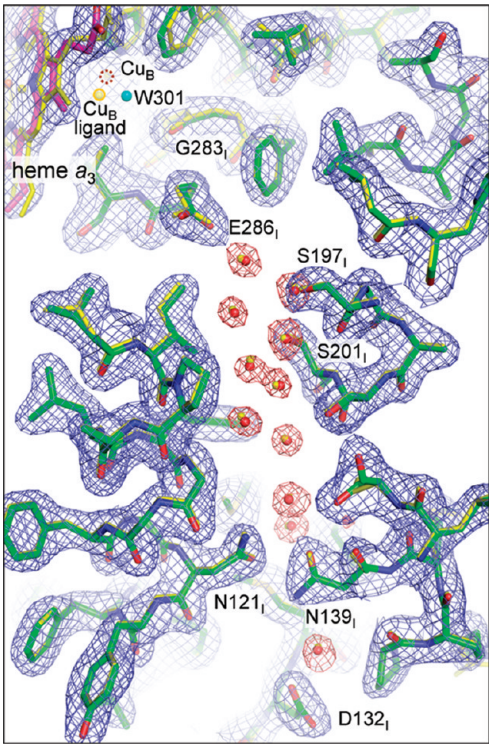

FIGURE 4: Comparison of the reduced vs oxidized structures in the D path. In the reduced structure, the amino acid residues are displayed in sticks and colored by atom type (C, green; O, red, N, blue), and heme a_3 is also displayed as sticks and colored by atom type (C, magenta; O, red; N, blue). Water molecules resolved in the D path are displayed as small red spheres. In this view, the Cu_B center is deep in the background and hardly visible, and its presence is highlighted by a brown dashed circle. $2F_o - F_c$ difference Fourier electron density map, contoured at 1.0σ, is colored dark red for regions surrounding the D path waters and blue for everywhere else. The oxidized structure is displayed in the same style as in the reduced structure and is colored yellow, except that the extra water (W301) resolved between the top of the D path and the binuclear center is shown as a cyan sphere. One of the ligands of W301 in the oxidized structure, temporarily assigned as an OH^- ligated to Cu_B, is not clearly visible in this view, and its presence is highlighted by a yellow circle and is labeled as Cu_B ligand in the figure.

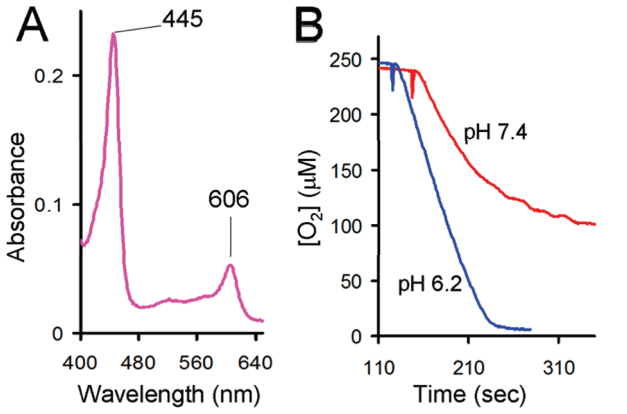

FIGURE 5: (A) Optical spectrum of redissolved reduced crystals of I−II *Rs*C*c*O. The spectrum is obtained by dissolving previously reduced crystals in buffer with added dithionite, showing native C*c*O characteristics. (B) Activity assays of redissolved reduced I−II *Rs*C*c*O crystals. Suicide inactivation of C*c*O is observed at pH 7.4 (red trace), with an initial velocity of 1067 e^-/s; this suicide inactivation is alleviated by lowering pH (pH 6.2, blue trace), with an initial velocity of 1680 e^-/s.

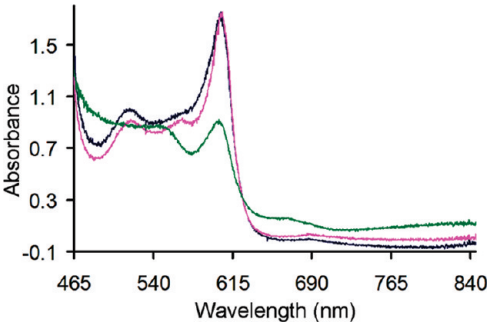

FIGURE 6: Spectral studies of irradiated reduced crystals. The blue spectrum was taken immediately after the irradiated, reduced crystal was transferred from liquid nitrogen into the soaking buffer that contained a small amount of dithionite to remove oxygen and prevent oxidation. The magenta spectrum was taken approximately 2 min after the crystal was soaked in the cryosolution supplemented with dithionite. The dark green spectrum was taken approximately 10 min after the soaking buffer was exchanged into fresh oxygenated buffer. The spectra that were recorded show normal characteristics of the native enzyme.

irradiation can have damaging effects on crystals. In the case of metalloproteins, there are additional concerns about maintenance of the redox state of the original crystal (*27*). By using a microspectrophotometer, we were able to investigate the spectral properties of single, reduced *Rs*C*c*O crystals after irradiation, and the results are shown in Figure 6. (Note that due to the optical density of the crystals, the Soret peak could not be reliably recorded in all of the spectral studies, and all of the spectra are presented in the range of 465−850 nm.) A normal reduced C*c*O spectrum was observed for crystals after data collection. Moreover, given time and fresh oxygenated soaking solution, the reduced crystal reoxidized and displayed a normal oxidized C*c*O spectrum.

DISCUSSION

It is still a major question in the field of cytochrome oxidase as to the mechanism of coupling of proton translocation to electron transport. A role for short- or long-range conformational changes has been proposed, linking the oxygen chemistry and redox changes in the metal centers to p*K* changes in proton transfer or loading sites and altered proton conducting water pathways (*8*, *18*, *38*−*41*). Trapping intermediates in catalytic reactions is difficult crystallographically, given the tendency of crystallization to favor the most stable conformation. Yet redox-dependent protein conformational changes have been directly observed in many heme proteins. In the classic example of hemoglobin, binding of oxygen to the reduced form, or allosteric effectors, elicits long-range changes in neighboring subunits (*42*). In bacterial nitrite reductase (cytochrome cd_1), the reduction of the active site heme d_1 leads to significant domain movement of the protein, as well as displacements of the heme *c* and heme d_1 groups (*43*). It is certainly the case that redox energy can be harnessed by protein conformational changes for chemical catalysis (*44*).

Redox-dependent conformational changes have also been observed in C*c*O. In the bovine mitochondrial C*c*O structure, unlike the *Rs*C*c*O, a change in position of Asp51 (bovine numbering; not conserved in *Rs*) was noted, along with rotation of the OH group of the hydroxyl farnesyl tail of the low-spin heme *a* some 110° away from its original hydrogen-bonding partner, $Ser382_I$ (bovine numbering; *Rs*, $Ser425_I$). This altered position is accompanied by a conformational change in a small patch of residues involving 380−382 (bovine numbering; *Rs*, 423−425) of subunit I (*45*). The movement of this latter patch of residues was also observed in the reduced structure of *Rs*C*c*O, as shown in Figure 1. However, the hydrogen bond between heme *a* farnesyl−OH and $S382_I$−OH that is broken in bovine C*c*O is not present in the *Rs*C*c*O oxidized structure, due to a different orientation of the heme *a* farnesyl tail that is not affected by the redox state.

Heme *a* and its precursor heme *o* both have long hydroxyl farnesyl tails and are always found in the active site of A-type heme copper terminal oxidases, such as the aa_3 and bo_3 oxidases. Therefore, it is likely that hemes *a* and *o* serve more purposes than merely binding the Fe ion to facilitate electron transfer, given the extra synthetic investment. One possible functional role could be to transmit conformational changes driven by the reduction of the Fe ion in the porphyrin ring, to extend its impact to nearby residues and facilitate proton transfer. Indeed, in two bacterial quinol oxidases, replacement of high-spin heme *a* or heme *o* with heme *b* leads to loss of enzymatic activity (*46*, *47*), while similar replacement of the low-spin heme apparently yields a functional enzyme (*48*).

Differences between the Reduced RsCcO Structure and Other Reduced Oxidases. The major redox-dependent changes we observed here, the displacement of heme a_3, the movement of nearby residues in helix VIII, and the new water molecules resolved between $T359_I$ and the binuclear center, have not been reported previously in C*c*O structures from other sources, including the bovine aa_3 oxidase (*29*, *38*), the *P. denitrificans* aa_3 oxidase (*28*), and the thermophilic bacterial ba_3 oxidase (*30*). Although the structure of the closely related bacterial aa_3 oxidase from *Pd* in the reduced state was reported to have no corresponding changes (*28*), the coordinates are not available in the PDB for direct comparison.

In the reduced bovine C*c*O structure, the distinctive redox-dependent conformational changes in residue D51 of subunit I (bovine numbering) and in the region of heme *a* led to a proposed new proton path (H path) and to a proton pumping mechanism that is centered on heme *a* and bypasses the heme−copper binuclear center (*29*, *38*). This mechanism has been supported by mutational analysis in mammalian cells (*49*), but neither mutagenesis studies with bacterial C*c*Os (*50*) nor the conformational changes reported here support the proposed bovine mechanism. The bovine and bacterial aa_3-type C*c*O share considerable sequence and structural homology, suggesting, but by no means proving, a similar mechanism for proton pumping. More studies will be required to understand the similarities and differences between these intricate energy conserving machines.

It is important to recognize that changes in crystal structures, or lack thereof, may be misleading since different conditions of crystallization may mask or favor certain conformational states. In either case, the true nature or extent of structural change may not be revealed. In this regard, the crystallization and reduction of bovine C*c*O crystals were performed at 4 °C, while bovine C*c*O is designed to work at a cow's body temperature of 40 °C. On the other hand, *Rs*C*c*O is designed to function well over a broader temperature range (10−40 °C). Studies with enzymes from the thermophilic bacteria show that there is a significant difference in their conformational flexibility at suboptimal temperatures compared to orthologous proteins from mesophilic organisms (*51*). In crystallography, the temperature is usually low and the ionic strength high, conditions that may favor a "ground state" conformation rather than a transient intermediate. This has been documented in the case of reduced and oxidized cytochrome *c* (*52*, *53*).

The changes observed in our study are not seen in reduced structures of the ba_3 oxidase from *T. thermophilis* (*30*). Aside from the likely difference in flexibility due to a 70 °C temperature optimum, this enzyme has been reported to lack a D path (*54*). If so, the mechanism and regulation of proton uptake may be different from that of the A-type oxidase and may not involve similar conformational changes.

The Route of Proton Uptake through the K Path. Previous studies indicate that the K path is responsible for the transport of one to two protons to the binuclear center during the initial metal reduction half of the catalytic cycle (O → R) (*8*, *12*, *55*). During the oxygen reduction phase of the cycle, the K path is expected to be closed (*19*) since evidence suggests that the D path alone is providing the protons during the P → F → O reactions (*8*, *9*, *56*). A conformational change of the $K362_I$ residue was proposed to break the hydrogen-bonded network that transports protons to the active site when oxygen binds at the

reduced binuclear center (*12*). Although only two water molecules, bonded to $K362_I$ and to $T359_I$, are resolved in the K path (*6*, *7*), computational MD analysis predicts the presence of more water in this channel, with the ability to form a hydrogen-bonded network (*57*).

In a molecular dynamics study of *Rs*C*c*O in the reduced state, a rotation of $T359_I$ was necessary to facilitate the formation of a hydrogen-bonded water chain from the $K362_I$−$S299_I$ region to heme a_3 farnesyl−OH (*57*). Interestingly, a bridging water molecule was also observed for an extended period of time between $Y288_I$−OH and heme a_3 farnesyl−OH, as observed in this study. Additional fixed water molecules were seen in the MD study leading from $Y288_I$−OH to the binuclear center itself, an observation also consistent with our crystal structure, albeit the exact positions of the water molecules in the two studies are different.

In another model (*18*), the strong hydrogen bond between the $Y288_I$−OH and heme a_3 farnesyl−OH is envisioned to be a gate controlling proton uptake through the K path. In the oxidized enzyme, the average distance between the two OH groups is 2.6 Å in the high-resolution crystal structures of bovine and *Rs*C*c*O, indicating that the gate is closed. During the initial reductive phase of the cycle, the covalently cross-linked $Y288_I$/$H284_I$ ligand of Cu_B is proposed to be transiently released from Cu_B and to undergo a conformational change that weakens the OH−OH hydrogen bond and opens the gate (*18*). In line with this prediction, one could postulate that the trigger for the conformational changes seen in the reduced crystal structure is the rearrangement of the His-Tyr Cu_B ligand, resulting in a loss of the OH−OH bond.

The observed conformational flexibility of helix VIII is also consistent with H/D exchange studies, which identify this region as largely solvent inaccessible in the oxidized state but becoming solvent accessible in the reduced state (*19*). In addition, computer modeling studies using the ProFlex program (*58*) suggest that this part of helix VIII is a relatively flexible region (L. Buhrow and L. Kuhn, unpublished work).

The Coordination between the D Path and the K Path. H/D exchange studies of *Rs*C*c*O in various intermediate states show little solvent accessibility for the majority of D path residues during the catalytic cycle (*19*). It is therefore perhaps not surprising that the hydrogen-bonded water chain connecting $D132_I$ to $E286_I$ is highly stable in many crystal structures, with the exception of mutants that are known to affect proton uptake, such as $D132A_I$ (Liu et al., unpublished results). Indeed, we observe no change in the D path water chain between the oxidized and reduced states of the wild-type *Rs*C*c*O.

$E286_I$, a key residue in the D path buried in the center of the membrane, was suggested by experimental and modeling studies to undergo conformational changes during the cycle, from a down position connected to the D path to an up position connected to the active site or to the D-propionate region above heme a_3 via newly formed water chains (*11*, *59*, *60*). This conformational change is suggested to be a D path gate (*61*). None of the crystal structures of C*c*O available so far have revealed the postulated additional water chains in this largely hydrophobic area. However, in the crystal structure of the two-subunit *Rs*C*c*O in the oxidized state, one water molecule is resolved in a position that could be part of such a chain (*7*) (Figure 4). The position of this additional water molecule is unique: it forms hydrogen bonds with the main-chain carbonyl oxygen of $G283_I$, as well as the Cu_B ligand OH^-. Interestingly, this additional water is also within hydrogen-bonding distance of the carboxyl oxygen of $E286_I$ when it is in one of its possible up conformations, making this water a candidate for bridging between the D path and the active site. This water could also connect to a proton exit route, via crystallographically unresolved water molecules. It is seen in a number of high-resolution *Rs*C*c*O structures in the oxidized state, including the deoxycholate-bound structure (PDB entry 3DTU) (*62*), as well as several structures of mutant forms (Liu et al., unpublished work).

However, this water disappears completely in the reduced structure, partly because one of its hydrogen-bonding ligands, the OH^- bound to Cu_B, is lost from the binuclear center. The disappearance suggests that the D path connection to the binuclear center is disrupted, at the same time as the K path connection is open. This implies a coordinated change in connectivity to the binuclear center with access controlled by the metal chemistry to prevent proton short circuiting between the two pathways.

Other Possible Explanations for the Observed Structural Changes in the Reduced RsCcO. Suicide inactivation is a typical behavior observed in C*c*O lacking subunit III. It is characterized by spontaneous and irreversible loss of activity during catalytic turnover (*37*). The underlying mechanism of suicide inactivation is not entirely understood at present, but it occurs when proton uptake through the D path (but not the K path) is impaired and not compensated for by proton backflow (*63*). As expected, the redissolved I−II subunit *Rs*C*c*O crystal exhibits suicide inactivation during steady-state turnover (*7*). It is reasonable to speculate that the observed structural changes in the reduced I−II subunit C*c*O could represent a form of the enzyme that is already inactivated or an intermediate en route to inactivation. However, when the reduced crystals are redissolved, they exhibit normal spectrum and oxidase activity (Figure 5). When the reduced crystals were reoxidized with ferricyanide, the displacement of heme a_3 and residue movements in helix VIII returned to normal. Most importantly, these structural changes were also seen in the reduced structure of the four-subunit *Rs*C*c*O, which does not show suicide inactivation. These lines of evidence demonstrate that this structure is not an artifact of the two-subunit enzyme. Similarly, as described in Results, the changes in conformation associated with reduction are not due to the inhibitory binding of Cd at the $E101_{II}$ site.

It should also be noted that reduction was carried out on crystals that were formed in the oxidized state. Thus it is possible that the changes seen are restricted by the crystal packing, which may limit the longer distance transmission of conformational effects.

In conclusion, the crystal structure of the *Rs*C*c*O in the fully reduced form shows novel structural changes compared to the oxidized form, which could simulate a physiological intermediate during the catalytic cycle. The major changes in the region of heme a_3 and helix VIII have not been reported in reduced structures of C*c*O from other sources but are consistent with evidence from computational and H/D exchange approaches. The observed changes minimally indicate significant flexibility in the region of heme a_3 and suggest a specific mechanism for gating of the K path and for alternating access to the D and K pathways.

ACKNOWLEDGMENT

We thank Dr. R. Michael Garavito from the Biochemistry and Molecular Biology Department, Michigan State University, for support and consultation. We thank beamline staff scientists Zdzislaw Wawrzak, Joseph Brunzelle, Spencer Anderson, and Keith Brister from LS-CAT, Ruslan Sanishvili (Nukri), Michael Becker, Nagarajan Venugopalan, Stephen Corcoran, Derek Yoder, Ward Smith, and Robert Fischetti from GM/CA-CAT, and Vukica Srajer and Yu-Sheng Chen from BioCARS, Advanced Photon Source, Argonne National Laboratory, for help during data collection. We thank Drs. Martyn A. Sharpe, Peter Nicholls, Steve Seibold, and Jonathan P. Hosler for helpful discussions and suggestions.

SUPPORTING INFORMATION AVAILABLE

Schematic drawing of the microspectrophotometer used for spectral analysis of the single crystal (Figure S1) and comparison of the distances between heme a_3 farnesyl−OH and $Y288_I$−OH, as well as the distances between Cu_B and heme a_3 Fe in different forms of *Rs*C*c*O (Table S1). This material is available free of charge via the Internet at http://pubs.acs.org.

REFERENCES

1. Hosler, J. P., Ferguson-Miller, S., and Mills, D. A. (2006) Energy transduction: proton transfer through the respiratory complexes. *Annu. Rev. Biochem. 75*, 165–187.
2. Brzezinski, P., and Gennis, R. (2008) Cytochrome *c* oxidase: exciting progress and remaining mysteries. *J. Bioenerg. Biomembr. 40*, 521–531.
3. Wikstrom, M., and Verkhovsky, M. I. (2007) Mechanism and energetics of proton translocation by the respiratory heme-copper oxidases. *Biochim. Biophys. Acta 1767*, 1200–1214.
4. Iwata, S., Ostermeier, C., Ludwig, B., and Michel, H. (1995) Structure at 2.8 Å resolution of cytochrome *c* oxidase from *Paracoccus denitrificans*. *Nature (London) 376*, 660–669.
5. Fetter, J. R., Qian, J., Shapleigh, J., Thomas, J. W., Garcia-Horsman, A., Schmidt, E., Hosler, J., Babcock, G. T., Gennis, R. B., and Ferguson-Miller, S. (1995) Possible proton relay pathways in cytochrome *c* oxidase. *Proc. Natl. Acad. Sci. U.S.A. 92*, 1604–1608.
6. Svensson-Ek, M., Abramson, J., Larsson, G., Tornroth, S., Brzezinski, P., and Iwata, S. (2002) The X-ray crystal structures of wild-type and EQ (I-286) mutant cytochrome *c* oxidases from *Rhodobacter sphaeroides*. *J. Mol. Biol. 321*, 329–339.
7. Qin, L., Hiser, C., Mulichak, A., Garavito, R. M., and Ferguson-Miller, S. (2006) Identification of conserved lipid/detergent-binding sites in a high-resolution structure of the membrane protein cytochrome *c* oxidase. *Proc. Natl. Acad. Sci. U.S.A. 103*, 16117–16122.
8. Konstantinov, A. A., Siletsky, S., Mitchell, D., Kaulen, A., and Gennis, R. B. (1997) The roles of the two proton input channels in cytochrome *c* oxidase from *Rhodobacter sphaeroides* probed by the effects of site-directed mutations on time-resolved electrogenic intraprotein proton transfer. *Proc. Natl. Acad. Sci. U.S.A. 94*, 9085–9090.
9. Adelroth, P., Ek, M. S., Mitchell, D. M., Gennis, R. B., and Brzezinski, P. (1997) Glutamate 286 in cytochrome aa_3 from *Rhodobacter sphaeroides* is involved in proton uptake during the reaction of the fully-reduced enzyme with dioxygen. *Biochemistry 36*, 13824–13829.
10. Busenlehner, L. S., Branden, G., Namslauer, I., Brzezinski, P., and Armstrong, R. N. (2008) Structural elements involved in proton translocation by cytochrome *c* oxidase as revealed by backbone amide hydrogen-deuterium exchange of the E286H mutant. *Biochemistry 47*, 73–83.
11. Hofacker, I., and Schulten, K. (1998) Oxygen and proton pathways in cytochrome *c* oxidase. *Proteins 30*, 100–107.
12. Branden, M., Sigurdson, H., Namslauer, A., Gennis, R. B., Adelroth, P., and Brzezinski, P. (2001) On the role of the K-proton transfer pathway in cytochrome *c* oxidase. *Proc. Natl. Acad. Sci. U.S.A. 98*, 5013–5018.
13. Adelroth, P., Gennis, R. B., and Brzezinski, P. (1998) Role of the pathway through K(I-362) in proton transfer in cytochrome *c* oxidase from *R. sphaeroides*. *Biochemistry 37*, 2470–2476.
14. Branden, M., Tomson, F., Gennis, R. B., and Brzezinski, P. (2002) The entry point of the K-proton-transfer pathway in cytochrome *c* oxidase. *Biochemistry 41*, 10794–10798.
15. Richter, O.-M. H., Duerr, K. L., Kannt, A., Ludwig, B., Scandurra, F. M., Giuffre, A., Sarti, P., and Hellwig, P. (2005) Probing the access of protons to the K pathway in the *Paracoccus denitrificans* cytochrome *c* oxidase. *FEBS J. 272*, 404–412.
16. Hosler, J. P., Shapleigh, J. P., Mitchell, D. M., Kim, Y., Pressler, M. A., Georgiou, C., Babcock, G. T., Alben, J. O., Ferguson-Miller, S., and Gennis, R. B. (1996) Polar residues in helix VIII of subunit I of cytochrome *c* oxidase influence the activity and the structure of the active site. *Biochemistry 35*, 10776–10783.
17. Sharpe, M. A., Qin, L., and Ferguson-Miller, S. (2005) Proton entry, exit and pathways in cytochrome oxidase: insight from conserved water, in *Biophysical and Structural Aspects of Bioenergetics* (Wikstrom, M., Ed.) pp 26−54, Royal Society of Chemistry, Cambridge, U.K.
18. Sharpe, M., and Ferguson-Miller, S. (2008) A chemically explicit model for the mechanism of proton pumping in heme−copper oxidases. *J. Bioenerg. Biomembr. 40*, 541–549.
19. Busenlehner, L. S., Salomonsson, L., Brzezinski, P., and Armstrong, R. N. (2006) Mapping protein dynamics in catalytic intermediates of the redox-driven proton pump cytochrome *c* oxidase. *Proc. Natl. Acad. Sci. U.S.A. 103*, 15398–15403.
20. Zhen, Y., Qian, J., Follmann, K., Hayward, T., Nilsson, T., Dahn, M., Hilmi, Y., Hamer, A. G., Hosler, J. P., and Ferguson-Miller, S. (1998) Overexpression and purification of cytochrome *c* oxidase from *Rhodobacter sphaeroides*. *Protein Expression Purif. 13*, 326–336.
21. Qin, L., Mills, D. A., Hiser, C., Murphree, A., Garavito, R. M., Ferguson-Miller, S., and Hosler, J. (2007) Crystallographic location and mutational analysis of Zn and Cd inhibitory sites and role of lipidic carboxylates in rescuing proton path mutants in cytochrome *c* oxidase. *Biochemistry 46*, 6239–6248.
22. Otwinowski, Z., and Minor, W. (1997) Processing of x-ray diffraction data collected in oscillation mode. *Methods Enzymol. 276*, 307–326.
23. Murshudov, G. N., Vagin, A. A., and Dodson, E. J. (1997) Refinement of macromolecular structures by the maximum-likelihood method. *Acta Crystallogr., Sect. D: Biol. Crystallogr. D53*, 240–255.
24. Bailey, S. (1994) The CCP4 suite: programs for protein crystallography. *Acta Crystallogr., Sect. D: Biol. Crystallogr. D50*, 760–763.
25. Emsley, P., and Cowtan, K. (2004) Coot: model-building tools for molecular graphics. *Acta Crystallogr., Sect. D: Biol. Crystallogr. D60*, 2126–2132.
26. Brunger, A. T., Adams, P. D., Clore, G. M., DeLano, W. L., Gros, P., Grosse-Kunstleve, R. W., Jiang, J.-S., Kuszewski, J., Nilges, M., Pannu, N. S., Read, R. J., Rice, L. M., Simonson, T., and Warren, G. L. (1998) Crystallography & NMR System: a new software suite for macromolecular structure determination. *Acta Crystallogr., Sect. D: Biol. Crystallogr. D54*, 905–921.
27. Pearson, A. R., Pahl, R., Kovaleva, E. G., Davidson, V. L., and Wilmot, C. M. (2007) Tracking X-ray-derived redox changes in crystals of a methylamine dehydrogenase/amicyanin complex using single-crystal UV/Vis microspectrophotometry. *J. Synchrotron Radiat. 14*, 92–98.
28. Harrenga, A., and Michel, H. (1999) The cytochrome *c* oxidase from *Paracoccus denitrificans* does not change the metal center ligation upon reduction. *J. Biol. Chem. 274*, 33296–33299.
29. Yoshikawa, S., Shinzawa-itoh, K., Nakashima, R., Yaono, R., Yamashita, E., Inoue, N., Yao, M., Fei, M. J., Libeu, C. P., Mizushima, T., Yamaguchi, H., Tomizaki, T., and Tsukihara, T. (1998) Redox-coupled crystal structural changes in bovine heart cytochrome *c* oxidase. *Science (Washington, DC) 280*, 1723–1729.
30. Liu, B., Chen, Y., Doukov, T., Soltis, S. M., Stout, C. D., and Fee, J. A. (2009) Combined microspectrophotometric and crystallographic examination of chemically-reduced and X-ray radiation-reduced forms of cytochrome ba_3 oxidase from *Thermus thermophilus*: structure of the reduced form of the enzyme. *Biochemistry 48*, 820–826.
31. Van Steelandt-Frentrup, J., Salmeen, I., and Babcock, G. T. (1981) A ferrous, high-spin heme a model for cytochrome a_3 in the dioxygen reducing site of cytochrome oxidase. *J. Am. Chem. Soc. 103*, 5981–5982.
32. Petersen, L. C. (1977) The effect of inhibitors on the oxygen kinetics of cytochrome *c* oxidase. *Biochim. Biophys. Acta 460*, 299–307.
33. van Buuren, K. J., Nicholls, P., and van Gelder, B. F. (1972) Biochemical and biophysical studies on cytochrome aa_3. VI. Reaction of cyanide with oxidized and reduced enzyme. *Biochim. Biophys. Acta 256*, 258–276.

34. Rich, P. R., and Breton, J. (2001) FTIR studies of the CO and cyanide adducts of fully reduced bovine cytochrome *c* oxidase. *Biochemistry 40*, 6441–6449.
35. Mills, D. A., Schmidt, B., Hiser, C., Westley, E., and Ferguson-Miller, S. (2002) Membrane potential-controlled inhibition of cytochrome *c* oxidase by zinc. *J. Biol. Chem. 277*, 14894–14901.
36. Aagaard, A., Namslauer, A., and Brzezinski, P. (2002) Inhibition of proton transfer in cytochrome *c* oxidase by zinc ions: delayed proton uptake during oxygen reduction. *Biochim. Biophys. Acta 1555*, 133–139.
37. Bratton, M. R., Pressler, M. A., and Hosler, J. P. (1999) Suicide inactivation of cytochrome *c* oxidase: catalytic turnover in the absence of subunit III alters the active site. *Biochemistry 38*, 16236–16245.
38. Tsukihara, T., Shimokata, K., Katayama, Y., Shimada, H., Muramoto, K., Aoyama, H., Mochizuki, M., Shinzawa-itoh, K., Yamashita, E., Yao, M., Ishimura, Y., and Yoshikawa, S. (2003) The low-spin heme of cytochrome *c* oxidase as the driving element of the proton-pumping process. *Proc. Natl. Acad. Sci. U.S.A. 100*, 15304–15309.
39. Behr, J., Hellwig, P., Mantele, W., and Michel, H. (1998) Redox dependent changes at the heme propionates in cytochrome *c* oxidase from *Paracoccus denitrificans*: direct evidence from FTIR difference spectroscopy in combination with heme propionate ^{13}C labeling. *Biochemistry 37*, 7400–7406.
40. Wikstrom, M., Verkhovsky, M. I., and Hummer, G. (2003) Water-gated mechanism of proton translocation by cytochrome *c* oxidase. *Biochim. Biophys. Acta 1604*, 61–65.
41. Quenneville, J., Popovic, D. M., and Stuchebrukhov, A. A. (2004) Redox-dependent pK_a of CuB histidine ligand in cytochrome *c* oxidase. *J. Phys. Chem. B 108*, 18383–18389.
42. Ciaccio, C., Coletta, A., De Sanctis, G., Marini, S., and Coletta, M. (2008) Cooperativity and allostery in hemoglobin function. *IUBMB Life 60*, 112–123.
43. Nurizzo, D., Cutruzzola, F., Arese, M., Bourgeois, D., Brunori, M., Cambillau, C., and Tegoni, M. (1999) Does the reduction of *c* heme trigger the conformational change of crystalline nitrite reductase?. *J. Biol. Chem. 274*, 14997–15004.
44. Williams, P. A., Fulop, V., Garman, E. F., Saunders, N. F., Ferguson, S. J., and Hajdu, J. (1997) Haem-ligand switching during catalysis in crystals of a nitrogen-cycle enzyme. *Nature 389*, 406–412.
45. Yoshikawa, S. (2005) Structural chemical studies on the reaction mechanism of cytochrome *c* oxidase, in *Biophysical and Structural Aspects of Bioenergetics* (Wikstrom, M., Ed.) pp 55−71, Royal Society of Chemistry, Cambridge, U.K.
46. Zickermann, I., Tautu, O. S., Link, T. A., Korn, M., Ludwig, B., and Richter, O. M. (1997) Expression studies on the ba_3 quinol oxidase from *Paracoccus denitrificans*. A bb_3 variant is enzymatically inactive. *Eur. J. Biochem. 246*, 618–624.
47. Saiki, K., Mogi, T., and Anraku, Y. (1992) Heme O biosynthesis in *Escherichia coli*: the cyoE gene in the cytochrome *bo* operon encodes a protoheme IX farnesyltransferase. *Biochem. Biophys. Res. Commun. 189*, 1491–1497.
48. Contreras-Zentella, M., Mendoza, G., Membrillo-Hernandez, J., and Escamilla, J. E. (2003) A novel double heme substitution produces a functional bo_3 variant of the quinol oxidase aa_3 of *Bacillus cereus*. Purification and paratial characterization. *J. Biol. Chem. 278*, 31473–31478.
49. Shimokata, K., Katayama, Y., Murayama, H., Suematsu, M., Tsukihara, T., Muramoto, K., Aoyama, H., Yoshikawa, S., and Shimada, H. (2007) The proton pumping pathway of bovine heart cytochrome *c* oxidase. *Proc. Natl. Acad. Sci. U.S.A. 104*, 4200–4205.
50. Lee, H.-m., Das, T. K., Rousseau, D. L., Mills, D., Ferguson-Miller, S., and Gennis, R. B. (2000) Mutations in the putative H-channel in the cytochrome *c* oxidase from *Rhodobacter sphaeroides* show that this channel is not important for proton conduction but reveal modulation of the properties of heme *a*. *Biochemistry 39*, 2989–2996.
51. Bae, E., and Phillips, G. N.Jr. (2004) Structures and analysis of highly homologous psychrophilic, mesophilic, and thermophilic adenylate kinases. *J. Biol. Chem. 279*, 28202–28208.
52. Sanishvili, R., Volz, K. W., Westbrook, E. M., and Margoliash, E. (1995) The low ionic strength crystal structure of horse cytochrome *c* at 2.1 Å resolution and comparison with its high ionic strength counterpart. *Structure 3*, 707–716.
53. Takano, T., and Dickerson, R. E. (1981) Conformation change of cytochrome *c*. II. Ferricytochrome *c* refinement at 1.8 Å and comparison with the ferrocytochrome structure. *J. Mol. Biol. 153*, 95–115.
54. Smirnova, I., Zaslavsky, D., Fee, J., Gennis, R., and Brzezinski, P. (2008) Electron and proton transfer in the ba_3 oxidase from *Thermus thermophilus*. *J. Bioenerg. Biomembr. 40*, 281–287.
55. Pecoraro, C., Gennis, R. B., Vygodina, T. V., and Konstantinov, A. A. (2001) Role of the K-channel in the pH-dependence of the reaction of cytochrome *c* oxidase with hydrogen peroxide. *Biochemistry 40*, 9695–708.
56. Brzezinski, P., and Adelroth, P. (1998) Pathways of proton transfer in cytochrome *c* oxidase. *J. Bioenerg. Biomembr. 30*, 99–107.
57. Cukier, R. I. (2005) A molecular dynamics study of water chain formation in the proton-conducting K channel of cytochrome *c* oxidase. *Biochim. Biophys. Acta 1706*, 134–146.
58. Jacobs, D. J., Rader, A. J., Kuhn, L. A., and Thorpe, M. F. (2001) Protein flexibility predictions using graph theory. *Proteins 44*, 150–165.
59. Puustinen, A., and Wikstrom, M. (1999) Proton exit from the heme-copper oxidase of *Escherichia coli*. *Proc. Natl. Acad. Sci. U.S.A. 96*, 35–37.
60. Seibold, S. A., Mills, D. A., Ferguson-Miller, S., and Cukier, R. I. (2005) Water chain formation and possible proton pumping routes in *Rhodobacter sphaeroides* cytochrome *c* oxidase: a molecular dynamics comparison of the wild type and R481K mutant. *Biochemistry 44*, 10475–10485.
61. Kaila, V. R., Verkhovsky, M. I., Hummer, G., and Wikstrom, M. (2008) Glutamic acid 242 is a valve in the proton pump of cytochrome *c* oxidase. *Proc. Natl. Acad. Sci. U.S.A. 105*, 6255–6259.
62. Qin, L., Mills, D. A., Buhrow, L., Hiser, C., and Ferguson-Miller, S. (2008) A conserved steroid binding site in cytochrome *c* oxidase. *Biochemistry 47*, 9931–9933.
63. Mills, D. A., Tan, Z., Ferguson-Miller, S., and Hosler, J. (2003) A role for subunit III in proton uptake into the D pathway and a possible proton exit pathway in *Rhodobacter sphaeroides* cytochrome *c* oxidase. *Biochemistry 42*, 7410–7417.